Visualizing translating dynamics in situ at high spatial and temporal resolution in eukaryotic cells

Jing Cheng[1], Chunling Wu[1], Junxi Li[1,2], Qi Yang[1,2], Xinzheng Zhang[1,2,3*]

[1]National Laboratory of Biomacromolecules, CAS Center for Excellence in Biomacromolecules, Institute of Biophysics, Chinese Academy of Sciences, Beijing 100101, China

[2] University of Chinese Academy of Sciences, 100049 Beijing, People's Republic of China.

[3] Center for Biological Imaging, CAS Center for Excellence in Biomacromolecules, Institute of Biophysics, Chinese Academy of Sciences, 100101 Beijing, China.

These authors contributed equally: Jing Cheng, Chunling Wu, Junxi Li.

* For correspondence: xzzhang@ibp.ac.cn

Summary

Cryo-electron microscopy can determine the structures of complexes within their native cellular environments. Because many of these complexes are highly dynamic in cells, characterizing their conformational changes is crucial for unraveling their biological functions. Here, we used translating ribosomes as a model system to investigate protein dynamic processes by GisSPA. We obtained 451,700 particles within two-days data collection from cryo-FIB milled *Saccharomyces cerevisiae* cells and solved the ribosome 60S region to 2.9 Å resolution. Multiple conformations with resolutions typically higher than 4 Å were identified by improving the 3D classification workflow. Some of these conformations revealed previously unobserved intermediates of peptidyl transfer and tRNA translocation. Thus, our work provides unprecedented high spatial and temporal resolution of the ribosome elongation cycle and demonstrates the power of GisSPA to visualize protein dynamics in atomic detail inside cells, highlighting its potential for studying structural dynamics in biological systems.

Introduction

Studying the conformational dynamics of protein machines by cryo-electron

microscopy (cryo-EM) is an important endeavor. In the past few years, structural studies of multi-conformations have been primarily achieved by in vivo single-particle analysis (SPA) with high resolutions readily obtained. However, simulating the biological environment in cells in vivo using SPA is challenging, resulting in issues such as not observing all macromolecular activities[1]. In situ dynamic structural studies of proteins in cells provide full complement of protein functional states compared to SPA, but the resolution of in situ protein structure determination is usually limited.

Protein synthesis performed by ribosomes is a complex process consisting of four steps: initiation, elongation, termination, and ribosome recycling. The process of incorporating each new amino acid into the nascent peptide chain during elongation involves multiple conformational rearrangements of the ribosome. Therefore, the conformational landscape of the translating ribosome represents an excellent example for investigating protein dynamics in situ. Using mRNA as a template, tRNA is responsible for base pairing with the mRNA codon, and ribosomes synthesize polypeptides from amino acids carried the ribosome-bound tRNAs. The peptidyl transferase center (PTC) is located in the large subunit of the ribosome, which is responsible for catalyzing the formation of peptide bonds and transferring the amino acids carried by tRNA to the growing peptide chain. Elongation factor 1 (eEF1A in eukaryotes) combined with GTP facilitates the transport of the aminoacyl tRNA to the A/T site, and elongation factor 2 (eEF2 in eukaryotes) assists in the translocation of the ribosome along the mRNA reading frame to ensure its accuracy. The tRNA at the A and P sites also translocate to the P and E sites respectively, and the vacated A site receives the aminoacyl tRNA required for the next round of peptide chain extension. Deacyl-tRNA at the P site is then released from the ribosome, and particular eukaryotes also require the involvement of elongation factor 3 (eEF3) in this process, such as *Saccharomyces cerevisiae* (*S. cerevisiae*)[2].

During ribosomal translocation, ribosomes, tRNA and mRNA undergo large-scale conformational changes. Some intermediate states have been analyzed by X-ray and cryo-EM (reviewed in[3]), but, limited by the complexity of eukaryotic systems, many in vivo studies have focused on bacteria. In addition, recent studies based on cryo-electron tomography (cryo-ET) have elaborated on cellular translation processes in eukaryotes[4,5] or prokaryotes[6]. However, these studies have only achieved high-resolution structural analysis of an averaged ribosome in different states, with the resolution of individual states limited by the number of particles used, resulting in an average resolution of 6 to7 Å, which is insufficient for atomic model building. In addition, these studies may not observe conformations with relatively low percentages when analyzing protein dynamics because of the low resolutions and the lack of particles.

Our previous work showed that GisSPA can solve high-resolution structures in cells with the complete stable PBS-PSII complex obtained in situ[7,8]. However, using GisSPA to analyze multiple conformations has not been explored. In this work, we investigated the eukaryotic ribosome of *S. cerevisiae* from cryo-FIB milled cells and determined 24 distinct in situ ribosome structures at resolutions ranging from 3.2 to

4.8 Å. Notably, most of these structures were in complex with elongation factors with several of these states previously not resolved. We reconstructed the elongation cycle with high spatial and temporal resolutions using these high-resolution structures. Overall, our work demonstrates that high-resolution in situ structural studies can provide more native complexes and reveal detailed biochemical processes. The data demand is very large when trying to achieve high spatial and temporal resolution by in situ structural analysis. Thus, analyzing a sufficient number of particles is crucial for capturing all conformations undergoing rapid biological processes, ensuring that high-resolution structural analysis of individual intermediates is achieved.

Result

In situ ribosome structure determination by GisSPA

S. cerevisiae cells were frozen on grids and thinned by cryo-FIB milling to visualize the various conformations of the eukaryotic ribosome during translation. Lamellae (Figure 1a) were tilted by 8° before data collection to compensate for the milling angle. A total of 3,702 micrographs (Figure 1b) were collected directly on the zero-degree-lamella from nine grids without tilt series. Ribosome particles with various conformations were recognized by taking the available cryo-EM map of the large ribosome subunit (60S) (EMD-6615)[9], which is relatively more homogeneous than the small subunit (40S), as the initial 3D template. The localization task was performed by generating 1,649 2D projections (ignoring the in-plane rotation) that uniformly covered the sphere model with a 5° angular step. The task was initially performed on 500 micrographs, and 7,043 ribosome particles were detected using the threshold of GisSPA as 6.8. Further local refinement by RELION[10] yielded a 5.9-Å resolution reconstruction. Then we performed a second round of localization on the whole dataset with the 60S segmentation of the 5.9-Å resolution map as the 3D model. Only frequencies from 1/400 $Å^{-1}$ to 1/8 $Å^{-1}$ were used in the calculations for both localization tasks and the overlapping parameter defined in GisSPA was set to three.

We obtained 808,736 potential particles from the 3,702 micrographs that met the new cutting threshold of 6.2. A round of 3D classification was carried out on the 808,736 particles using RELION. Among them, 451,700 particles were classified into true detections. By combing with CTF refinement and Bayesian polishing, we achieved an overall resolution of 2.9 Å for 60S region (Figure 1c) using these particles. The high-resolution map revealed well-resolved ribosomal RNA (rRNA) bases and ribosomal protein amino acid side chains (Figure 1d).

Multi-conformations 3D classification

The local resolution of 80S varies noticeably between the 40S and 60S regions because of structural dynamics, so individual conformation should be identified. Different from single particle data, the signal-to-noise ratio of 2D particles in cells is quite low in the low-resolutions range. Therefore, high-resolution data must be involved in 3D classifications and only very local refinement is allowed during classification.

To identify the multiple states in translation and to study structural heterogeneity, we performed 3D classifications based on the well-refined 80S ribosome particle without alignment using masks including regions with heterogeneities via cryoSPARC[11]. The parameter "Target resolution" in 3D classification, which corresponds to the resolution range for calculating, must be carefully designed according to the data characteristics, and 6 to 8 Å was used in this study. The 3D classification analysis yielded different conformations for the 40S, tRNAs, eEF2, eEF3 and L1 stalk. The particle images were separated into special states (Figure 2, Supplementary Figures S1 and S2abc) and the translation elongation cycle was reconstructed according to the assignment of the 3 elongation factors (eEF1A, eEF2 and eEF3) and locations of tRNAs binding to the ribosome (Figure 2a). Eleven states of these are main conformations making up the elongation cycle (Figure 2a and Supplementary Movie 1), and three of the main conformations can be further divided into nine sub-conformations according to the presence of eEF3 (Figure 2e and Supplementary Figure S2bc).

Of the eleven main conformations of the cycle (Figure 2a), two states: "A/T, P" (states 1) and "A/T, P, E" (state 8) standing for ribosome undergoing the mRNA decoding process, four states presenting the stepwise native peptide transfer process (state 2a-2d) and three classical states: "aa/P, p/E"(states 4), "ap/P, p/E" (state 6) and "P, E" (state 7) and two new intermediate states (states 3 and 5) belonging to tRNA translocation were obtained. The 40S head and body rotations in each state were measured (Figure 2c). Four additional states were attributed to the fast-transformed intermediates or not part of the classical cycle and are listed separately in Figure 2d. The number of particles accounted for by each state is listed in Supplementary Table 1.

Conformational rearrangement of eEF2 on ribosome from compact to fully-extended

Our results showed that eEF2 exhibited two distinct conformations throughout the elongation cycle: compact and extended (Figure 3a). The extend eEF2 conformation has been widely studied previously, whereas less research has been done on compact eEF2. A ribosome crystal structure with a compact EF-G in prokaryote has been reported[11], however, no similar structures were obtained in eukaryotic. We docked the six domains of eEF2 in to the EM maps independently (Supplementary Figure S3abc). We found that the compact eEF2 is in complex with the partially rotated ribosome in the "A, P" state (Figure 2a) and the extended eEF2 interacts with the ribosome by two mechanisms: less-extended manner and fully-extended manner. Less-extended eEF2 binds to the fully rotated ribosome in the "aa/P, p/E" state (state 4) and fully-extended eEF2 was presented in the following three translocation states (states 5,6 and 7). By superimposing the two extended structures (Supplementary Figure S3d), we found that unlike the previous study on *Mycoplasma pneumoniae*[6], eEF2 maintains its conformation from less-extended to fully-extended with a Ca RMSD of 1.8 Å, which is consistent with previous study by SPA on prokaryotes[12].

We compared the arrangement of eEF2 domains of compact eEF2 and extend eEF2

by superimposition (Figure 3b), and the results showed that four domains, domains I, II, III and G, are relatively fixed among each other, and domains IV-V are fixed as another rigid body. Domain I-G maintain their arrangements, but domains IV-V undergo a rotation of approximately 40˚ around an axis of the junction between them. This rotation causes domain IV of compact eEF2 to extend about 48 Å, mostly towards the A site of 40S, and domain V shifts approximately 23 Å mostly to be primarily closer to 40S. This conformational rearrangement of eEF2 domains is similar to previous observations in prokaryote[12], but the rotation and displacement differ.

Following the elongation cycle (Figure 2a), compact eEF2 initially binds to the partially-rotated ribosome belonging to peptidyl transfer (state 2c), indicating that the partially rotated ribosome state in the "A, P" state may be the substrate of compact eEF2. When the tRNA began to translocate, compact eEF2 transformed and then complexed with the "aa/P, p/E" ribosome (state 4) in less-extended manner, where domain IV does not overlap with A site on 40S as previously resolved in situ[6,12]. With the movement of tRNAs along mRNA, eEF2 extended towards the A site and reached the fully-extended manner in the newly-resolved translocation state 5 (Supplementary Figure S4). eEF2 maintained itself until the disassociation when the 40S rotated back to the unrotated state.

To understand the changes of interaction between eEF2 and ribosome in the transformations above[12], we used 60S as the reference to analyze the shifts and rotations of eEF2 domains relative to ribosome. From compact to less-extended, eEF2 domains I-III rotated ~30˚ and domains IV-V rotated ~60˚, yielding a movement of ~80 Å for domain IV (Figure 3c). From less-extended to fully-extended, eEF2 domains have a monolithic rotation of ~15˚, leading to domain IV of state 6 being extended by mostly ~20 Å towards the A site on 40S (Figure 3c).

As eEF2 binds to ribosomes from compact conformation to fully-extended manner, domain 5's interaction with P stalk and A3027 of 25sRNA is maintained (Supplementary Figure S5). By aligning domain V of extended eEF2 with compact eEF2 on ribosome in state 2c, we found that steric hindrance formed by the arrangement of ribosomal proteins and rRNA, which leads to a clash of the domains I and G with the 60S (Supplementary Figure S6a), hinders the formation of extended eEF2. When the ribosome transitions to state 4, P stalk closes by ~7 Å towards tRNA (Supplementary Figure S6b) and 40S body rotates by 4 degrees, allowing the formation of eEF2 in the extended conformation.

Conformational rearrangement of eEF3 throughout the elongation

We resolved two conformations of eEF3 and refer to the conformations as stably bound to the fully rotated ribosome (conformation 1) and stably bound to the unrotated ribosome (conformation 2) (Figure 4a). Conformation 2 is essentially the same state obtained from the single-particle analysis, i.e., the closed conformation[13], but conformation 1 has not been resolved previously. The local resolution of conformation 1 is lower (Supplementary Figure S7) because of its inherent flexibility. We docked the domains of eEF3 into the EM density (Supplementary Figure S8ab)

and called this the open conformation as opposed to the closed conformation. The main difference between the two conformations is the arrangement of the ABC1 and ABC2 domains (Figure 5b), which are in complex with ATP[13]. Throughout the elongation cycle, the ribosome does not bind eEF3 during the peptide transfer process. Therefore, we concluded that the open conformation of eEF3 binds to the ribosome when 40S reaches the fully rotated state, then closed-eEF3 dissociates from the ribosome prior to peptide transfer. Open conformation eEF3 binding to the ribosome promotes the reverse rotation of 40S, thereby facilitating the unrotated 80S. We observed that when 40S reached the partially-rotated conformations, the binding of eEF3 to the ribosome became unstable, leading to poor eEF3 density, and the conformation of eEF3 was observed to transform to the closed conformation in "ap/P, p/E" state (state 6) (Supplementary Figure S8cd).

The conformational change of eEF3 from closed to open implies the hydrolysis of ATP[13]. The binding of closed-eEF3 to the ribosome is stabilized when 80S returns to its unrotated state. During mRNA decoding, closed-eEF3 gradually weakens and finally disassociates from 80S before the peptidyl-transfer step (Figures 2e and 4c). Our structures showed that eEF3 favored the unrotated ribosome states, which is consistent with SPA findings by SPA[13]. However, there are some differences. One difference is that the release of the E-site tRNA didn't require the opening of L1, as we observed that even after E-site tRNA release, L1 remains closed in the part of ribosomes in "A/T, P" state (Supplementary Figure 2a). Another one is that the unrotated ribosome in classical "A, P" state (state 2a) didn't bind eEF3, while the fully-rotated ribosome (states 3 and 4) can bind eEF3 in open conformation.

Due to the presence of eEF3, ribosome of *S. cerevisiae* shows more conformations related to the binding, the conformational change and the disassociation of eEF3 than other species, thus making up more complex dynamic translation processes (Supplementary Movie 2).

eEF3 disassociating is accompanied by L1 closing during mRNA decoding

In the overall cryo-EM map of the "A/T, P" state, the density of eEF3 was essentially smeared, implying a relatively low occupancy of eEF3 or a very flexible eEF3 bound state. Therefore, a round of 3D classification focusing on the eEF3 region illustrated the 3D variability of eEF3 in the "A/T, P" state with the identification of four substates (Figure 2e): the stable binding to 80S state (state 1a, 20%), the less-flexible binding state (state 1b, 37%), the more-flexible binding state (state 1c, 19%) and the disassociated state (state 1d, 24%), where eEF3 may disassociate from the 80S. In the stable binding state, the L1 stalk of 80S adopted the open state, whereas, in the disassociated state, L1 switched to the closed state. The open state of L1 allows the release of the E-site tRNA and must close after this release. Thus, the movement of L1 with eEF3 shows that the transition from stable binding to disassociation of eEF3 is sequential. This transition was verified by classifying the particles into three classes according to the state of the L1 stalk: open state, intermediate state and closed state (Supplementary Figure S2a). We then classified eEF3 on each L1 state, with the percentage of the stable eEF3 binding state calculated

as 73%, 26% and 0%, respectively. We also analyzed the occupancy of eEF3 in the "A/T, P, E" state, revealing that eEF3 also has these three states (Supplementary Figure S2b) of stable binding (state 8a, 51%), flexible binding (state 8b, 23%) and unbound (state 8c, 26%).

The complete native peptidyl transfer process

Deep classifications on particles in the "A, P" state focused on 40S and eEF2 binding regions resulted in seven different conformations. Among these, six states (states 2a, 2b, 2c, 2d, state 2e and 2f) were associated with peptidyl transfer. The remaining state (state 9) containing 3.3% of ribosome particles with heterogeneities in the 60S and 40S regions (Supplementary Figure S9), probably does not belong to the reconstructed elongation cycle (Figure 2ab).

During peptide bond formation, the nascent peptide chain is transferred from the P-site tRNA to the newly incorporated A-site tRNA in the "A, P" state. Although, the 3D classification was not focused on PTC, the resulted six classes represented peptide transfer process according to the PTC. Among the six states, four states (state 2a-d) represented the known peptidyl transfer process, whereas one state (state 2e) appeared to not belong to this process and another state (state 2f) is probably to be an intermediate state between state 2a and state 2b. In the unrotated state 2a, the density of the A-site tRNA elbow was poorer than that of the anticodon stem-loop and the CCA of the A-site tRNA was not observed in the PTC. The nascent peptide chain is attached to P-site tRNA. These features in state 2a suggest that this state represents the pre-peptidyl transfer state. The 40S is then rotated by ~6˚ in state 2b. This rotation may facilitate the accommodation of A-site tRNA[14]. The nascent peptide chain is still connected to P-site tRNA at this step (Figure 5a), indicating that peptidyl transfer is not completed upon accommodating A-site tRNA. When the CCA of the A-site tRNA inserts into the PTC, the known peptide chain nucleophilic attack by the incoming free α-amino group onto the carbonyl carbon would break the acyl linkage between the carbonyl carbon and the 3' hydroxyl of the P-site tRNA[15] and form the peptide bond between the carbonyl carbon and the amino nitrogen. An intermediate state (state 2c) was observed during peptide bond formation (Figure 5bc). In this intermediate state, the peptide chain was not connected to either A-site tRNA or P-site tRNA at a contour value of 2.6 RMSD. Decreasing the value to 1.8 RMSD revealed the peptide chain connected to the two tRNAs simultaneously (Figure 5c), and we are sure that it can't be a mixture of states 2b and 2d, suggesting that this intermediate represented the tetrahedral intermediate of the nucleophilic attack. Additionally, the density of the CCA end of A-site tRNA was poorer than in states 2b and 2d, and the free amino acid in state 2c seemed to have a slight shift relative to state 2b (Supplementary Figure S10). eEF2 in its compact conformation[5,11] was bound to the partially-rotated ribosome in state 2c. The peptide chain was successfully transferred from P-site tRNA to A-site tRNA at state 2e (Figure 5d). The CCA end of P-site tRNA was observed to interact in the PTC with G2620, G2621 and A2820 and that of A-site tRNA interacted with G2922, U2923, U2924 and U2953 (Supplementary Figure S11).

In state 2e, the 40S subunit was observed in its unrotated conformation. In this state, the nascent peptide chain was not connected to the P-site tRNA nor the A-site tRNA. Instead, the peptide chain interacted with U2954 and U2955 of the 25S RNA (as shown in Figure 5e). Simultaneously, the CCA end of A-site tRNA and the amino acid were unresolved within the PTC. We also observed the presence of a compact eEF2 bound to the ribosome in this particular state.

In addition, extra densities (sequence 9-21) belonging to RPS25A protein, which has not been modeled previously, were clearly resolved in the partially rotated ribosome in the peptide transfer process (Supplementary Fig. S12). We used Alphafold1 to complete the RPS25A structure, and the extra densities were predicted to be a helix, which matches our cryo-EM densities. This helix extends over P-site tRNA and interacts with A-site tRNA (Supplementary Fig. S12).

Three classical and two newly-resolved intermediates describing the sequential tRNA translocation

The density of compact eEF2 became smeared after the formation of the peptide bond, indicating that the tRNAs must undergo translocation along the mRNA once the bond is formed. This translocation is necessary for the next codon to enter the A-site and initiate the subsequent translation cycle. Before the “aa/P, p/E” state (state 4), an intermediate (state 3) with a fully rotated 40S body was resolved, where the 40S body rotated at most by ~10˚ and the 40S head swiveled slightly by ~2˚. Moreover, the deacyl- tRNA already left the P site, but the peptidyl-tRNA was still in A-site with smeared elbow and CCA densities. In the “aa/P, p/E” state (state 4), ~52% of particles in this state include bound eEF3, whereas the remaining particles appear to not bind stable eEF3 (Supplementary Figure 2). eEF2 adopts a less-extended manner in this state, where domain IV does not overlap with the 40S A-site because the A-site tRNA is occupied, as described above. Another intermediate state (state 5) positioned between the “aa/P, p/E” and “ap/P, p/E” (state 6) states was identified, where the 40S body had a reverse rotation by ~3˚ and the 40S head swiveled ~14˚. The deacyl-tRNA and peptidyl-tRNA are similar to state 3 with stable deacyl-tRNA and flexible peptidyl-tRNA. In the “P, E” state (state 7), the peptidyl-tRNA reached the P-site and the deacyl-tRNA came to E site. These five intermediates revealed the sequential movement of tRNAs, with the deacyl-tRNA moving first, followed by the peptidyl-tRNA.

Discussion

In this study, we obtained 451,700 ribosomes within two days’ data collection in exponentially growing *S. cerevisiae* cells to resolve the dynamic process of ribosome elongation cycle at near atomic resolutions. To reach a similar amount of data, cryo-ET needs data collection for about two months. The large dataset not only increased the resolution of ribosome at each state, but also helped to capture the intermediate state whose occupancy is as low as ~1%. Therefore, In the study of protein dynamic processes that require a large amount of data, GisSPA has shown

great advantages over cryo-ET with high data acquisition throughput. In addition, with similar characteristics with low occupancy intermediates, our results indicated that in situ studies of proteins with low abundance like 1% of cytoplasmic ribosome in *S. cerevisiae* cells are also applicable by GisSPA.

The single large subunit and ribosomal conformations belonging to the initiation and termination states were absent in our results, while we have successfully identified conformations at a percentage of 1.5%, thus the absent states in our study present lower percentages than 1.5% in cells.

The most populated translation-elongation states of the cytosolic *S. cerevisiae* ribosome were the mRNA decoding and peptidyl-transfer steps. The changing conformational states during the mRNA decoding process are interspersed with the dissociation of eEF3, the closing of the L1 stalk, and the recognition of tRNA. We reconstructed the process of L1 closure and eEF3 dissociation, however, we faced challenges in distinguishing the different conformations involved in the mRNA decoding process. The transitions between these conformations are likely to occur rapidly, which made it challenging to capture distinct structures for each state. As a result, we obtained an average conformation representing an ensemble of conformations during the decoding process. Unlike the repeating conformational changes during decoding, peptide transfer is a unidirectional process, and thus we successfully identified the six distinct states belonging to the peptidyl transfer step.

Hydrolysis of GTP (ATP for eEF3) occurs when the elongation factors maintain ribosome translation, along with conformational changes depending on whether they are bound to GTP (ATP for eEF3) or GDP (ADP for eEF3). eEF3 contains two ATP-binding domains, thus carrying two ATP molecules. One ATP hydrolysis occurs concomitantly with the 40S reverse rotation,[13] leading to the conformational change to eEF3. The opening of the L1 stalk may be prompted by the hydrolysis of the second ATP[13], or driven by the 40S reverse rotation. The second ATP hydrolysis may contribute to the disassociation of eEF3 from the ribosome, where eEF3 binding is destabilized before disassociating. If this were the case, the second ATP hydrolysis causes a conformational change to eEF3 that disrupts the interaction interface between eEF3 and the ribosome, leading to eEF3 dissociating from the ribosome.

Method details

Cell culture

Saccharomyces cerevisiae strains BY4741 were inoculated in YPD medium overnight at 30 °C to an OD600 of 0.6 ~ 0.8. The cells were collected and resuspended in the same medium, and the concentration of the suspension was adjusted to an OD600 of 2.

Cryo-EM sample preparation and FIB milling

3 μL *S. cerevisiae* cells were applied to a glow-discharged copper Quantifoil 200 mesh R1.2/1.3 grid. Before 30s pre-blotting the grid was plunge-frozen into liquid

ethane using a Leica EM GP (Leica Microsystems) with 6 ~ 8 s back-side blotting at 16 □ with the chamber at 70% humidity.

Cryo-lamellae were prepared by cryo-FIB milling using the Aquilos-2 FIB-SEM microscope (Thermo Fisher Scientific). Before milling, samples were sputter-coated with metallic platinum for 10s with 15 mA beam current then coated with organo-platinum for 6s through the gas-injection-system (GIS) and coated metallic platinum for 10s again with the same settings. Lamellae were rough milled to ~300 nm using a decreasing Ga+ ion beam from 0.3 nA to 50 pA with a milling angle of 8°. 10 pA ion beam was used for the final polish to obtain a final ~ 150 nm thickness.

Cryo-EM data acquisition and image processing

Cryo-lamellae were collected by applying a single particles data collection method using FEI Titan Krios G3 (Thermo Fisher Scientific) equipped with a Gatan GIF K2 camera (Gatan, Icn.). Before collection, an offset start angle of 8° was set to compensate for the milling angle, ensuring that the lamellae perpendicular to the electron beam details refer to previous description[7,8]. Data collection was performed with SerialEM[16] and the beam-image shift data collection method[17] using a nominal magnification of 105,000 with a calibrated pixel size of 0.66 Å/pixel at super-resolution mode.

Two sets of dose rate were used during data collection, 219 micrographs were irradiated by 35 e^- and dose-fractionated to 40 frames, and the rest were collected with a total dose of 50 e^- and dose-fractionated to 50 frames.

The energy slit width was set to 20 eV and the nominal defocus was set between −0.8 to −1.2 μm. Motion correction was done by MotionCorr2[18] and micrographs were dose-weighted and binned with a factor of 2.

Structure determination by GisSPA

The CTF parameters of micrographs were estimated by CTFfind4[19] in RELION, then the micrograph file in “star” format was converted to “lst” format for the detection task. The 60S large subunit structure of yeast (EMD-6615) was used as the initial 3D model in GisSPA. We performed the initial detection task on the first 500 micrographs with overlapping parameter *k* as 3 and output score threshold as 6.8, resulting in 7043 particles in total. A round of local refinement on these particles yielded a structure of 80S at a resolution of 5.9 Å. To improve detection efficiency, we segmented the 60S from the new reconstructed map and used it as the template in GisSPA. To remove duplicated detections, potential particles within translational distance of ~10.6 angstroms and Euler distance of 8 degrees were merged as one particle.

808,736 potential particles from the 3,702 micrographs were kept after removing repeats. The particle file in “lst” format was converted back to “star” format for particle extraction in RELION. Particles were 2-binned extracted with a boxsize of 200, after implementing a round of 3D classification using the 3D model in detection as the initial model and the lowpass filter was set to 20 Å, ~56% of the particles

including the 40S density were selected and the rest showing bias features were throwed (Supplementary Fig. S1). Since the cryo-EM data on each grid was collected individually, we divided them in to 9 optical groups for the following refinements. 2 rounds of CTF parameters refinements, 1 round of beam tilt estimation and 2 rounds of local orientational and translational refinements were performed, the resolution was estimated as 3.0 Å in 60S region. To further improve the resolution, a round of Bayesian polishing was carried out, and another round of local refinement was applied to the polished particles, and the resolution in 60S region was improved to 2.9 Å.

3D classification and refinement

Ribosome 3D classifications were accomplished by CryoSPARC[20] with the imported refined particles from RELION3.2. First, focused classification with a smooth shape mask covering the A-, P-, E-site tRNA positions was performed. This resulted in four major classes with different tRNA occupancies: “A/T, P” (150,024 particles), “A, P” (193,692 particles), “A/T, P, E” (37,868 particles), “P, E” (62,528 particles) and “A” (7,588 particles). In the second round, we continued to classify particles belonging to “P, E’ class focused on 40S region, and this resulted in four tRNA translocation classes divided from “‘P’, ‘E’” class: “aa/P, E” (state 4), “ap/P, E” (state 6), “P, E” (state 7) and one translocation intermediate state (state 5) located between “aa/P, E” and “ap/P, E” states (Supplementary Fig. S1).

We found densities with lower occupancy presented in the P stalk binding site in the “A, P” state, so a third round of classification focused on the P stalk binding site was carried out on particles in “A, P” state, resulting in empty binding site class, compact eEF2 stable binding class and compact eEF2 density scattered class. Each class showed flexibilities in 40S region, therefore, a classification focused on 40S region was performed on each class. Particles were further classified into the following states: unrotated 40S without compact eEF2 binding (state 2a), rotated 40S without compact eEF2 binding (state 2b), rotated 40S with compact eEF2 stable binding (state 2c), rotated 40S with flexible compact eEF2 density (state 2d), unrotated 40S with stable compact eEF2 binding (state 2e), an intermediate state (state 2f) located between state 2a and state 2b and an intermediate class (state 3) positioned between “A, P” and “aa/P, p/E” states. In addition, 14,925 particles (state 9) belonging to “A, P” state had a lower resolution of 4.8 Å than other classes within similar particles, showing severe flexibilities in 40S region, and 7,588 particles only contain a tRNA in A-site (state 10) with 40S partially rotated similar to state 2b and state 2c.

To investigate the occupancies of eEF3 in class1, state 4 and state 8, 3 rounds classifications with a soft mask focus on eEF3 region were individually performed on the particles in three classes, resulting in stable eEF3 (class 1a, state 4a and state 8a), flexible eEF3 (class 1b, 1c and state 8b) and smeared eEF3 (class 1d, state 4b and state 8c). Classifications of particles in “A/T, P” state focused on L1 stalk were performed with a soft mask including regions of L1 stalk.

The masks used above were generated by *relion_mask_creation* command

implemented in RELION[10], and the input maps were segmented from the overall reconstruction in Chimera and low-passed to 20 Å.

Model building

The *S. cerevisiae* 60S subunit model was built based on the crystal structure (PDB:4V88). It is split into separate rRNA and protein parts and fit into the cryo-EM density. The non-rotated 40S subunit part was built based on the PDB ID 7OSM. For rotated 40S, PDB ID 7B7D was used. In addition, the refinement of PTC in 25S rRNA model refers to the 2.4 Å crystal structure (PDB :8CVJ). Alphafold1 was used to complete the RPS25A structure.

The eEF1A model was derived from the cryo-EM structure (PDB: 5LZS). Using PDB ID 2P8W as a template to build the elongated conformation of eEF2, the compact conformation of eEF2 needs to rigid-body-fit the six domains divided as previously described[21] (domain I \ domain G\ domain II \ domain III \ domain IV \ domain V) into the cryo-EM map by UCSF Chimera[22]. Another model (PDB:1N0V) is used for the rearrangement of the eEF2 compact conformation. The previous eEF3 model (PDB: 7B7D) was separated into 5 domains (HEAT \ 4HB \ ABC1 \ ABC2 \ CD)[2] that were fitted to cryo-EM map separately as rigid body in Chimera. The tRNA comes from (7B7D), and the aminoacyl-tRNA model was derived from PDB ID 8CVJ. The mRNA was built using PDB ID 6XHW as template. The nascent peptide was built de novo by constructing a poly-alanine sequence.

These domains fitted into each electron density map as rigid bodies in Chimera via fit in map function. Then manual adjust separate domains by real space refine and merge into a whole model in Coot[23]. The ribosome model is further refined by iterating in Coot and Phenix[24]. Validation was obtained using MolProbity7[25].

Acknowledgments

We thank L. Kong for cryo-EM data storage and backup. The project was funded by the National Natural Science Foundation of China (31930069 and 32150010), the Strategic Priority Research Program of the Chinese Academy of Sciences (XDB37040101), the National Key R&D Program of China (2021YFA1301501) and the Key Research Program of Frontier Sciences at the Chinese Academy of Sciences (ZDBS-LY-SM003).

Author contributions

X.-Z.Z. supervised the project. C.-L.W. and J.-X.L. prepared the *Saccharomyces cerevisiae* cells, milled the cells to cellular lamellae by cryo-FIB and collected the cryo-EM Data. J.C. performed the data processing and conducted the analysis. J.-X.L. conducted the model buildings. X.-Z.Z., J.C., C.-L.W. and J.-X.L. wrote the initial draft, and all authors contributed to the discussion of the results and revision of the manuscript.

Declaration of interests

The authors declare no competing interests.

Data and code availability

The electron density maps have been deposited to the Electron Microscopy Data Bank (EMDB): EMD-XXXXX, EMD-XXXXX, …, which are publicly available as of the date of publication. The atomic coordinates and structure factors have been deposited to the Protein Data Bank (PDB): XXXX, XXXX, …, which are publicly available as of the date of publication. The raw cryo-EM micrographs and particles used in this study have been deposited to the Electron Microscopy Data Bank (EMDB) under accession numbers XXXXX.

References

1. Dunstone, M. A. & de Marco, A. Cryo-electron tomography: An ideal method to study membrane-associated proteins. *Philosophical Transactions of the Royal Society B: Biological Sciences* **372**, (2017).
2. Andersen, C. B. F. *et al.* Structure of eEF3 and the mechanism of transfer RNA release from the E-site. *Nature* **443**, 663–668 (2006).
3. Korostelev, A. A. The Structural Dynamics of Translation. *Annu Rev Biochem* **91**, 245–267 (2022).
4. Gemmer, M. *et al.* Visualization of translation and protein biogenesis at the ER membrane. *Nature* **614**, (2023).
5. Hoffmann, P. C. *et al.* Structures of the eukaryotic ribosome and its translational states in situ. *Nat Commun* **13**, (2022).
6. Xue, L. *et al.* Visualizing translation dynamics at atomic detail inside a bacterial cell. *Nature* **610**, 205–211 (2022).
7. Cheng, J. *et al.* Determining protein structures in cellular lamella at pseudo-atomic resolution by GisSPA. *Nat Commun* **14**, (2023).
8. You, X. *et al.* In situ structure of the red algal phycobilisome–PSII–PSI–LHC megacomplex. *Nature* (2023) doi:10.1038/s41586-023-05831-0.
9. Wu, S. *et al.* Diverse roles of assembly factors revealed by structures of late nuclear pre-60S ribosomes. *Nature* **534**, 133–137 (2016).
10. Zivanov, J. *et al.* New tools for automated high-resolution cryo-EM structure determination in RELION-3. (2018) doi:10.7554/eLife.42166.001.
11. Lin, J., Gagnon, M. G., Bulkley, D. & Steitz, T. A. Conformational Changes of

552 Elongation Factor G on the Ribosome during tRNA Translocation. *Cell* **160**,
553 219–227 (2015).
554 12. Carbone, C. E. *et al.* Time-resolved cryo-EM visualizes ribosomal translocation
555 with EF-G and GTP. *Nat Commun* **12**, 7236 (2021).
556 13. Ranjan, N. *et al.* Yeast translation elongation factor eEF3 promotes late stages of
557 tRNA translocation. *EMBO J* **40**, e106449 (2021).
558 14. Loveland, A. B., Demo, G. & Korostelev, A. A. Cryo-EM of elongating ribosome
559 with EF-Tu•GTP elucidates tRNA proofreading. *Nature* **584**, 640–645 (2020).
560 15. Tirumalai, M. R., Rivas, M., Tran, Q. & Fox, G. E. The Peptidyl Transferase Center:
561 a Window to the Past. *Microbiology and Molecular Biology Reviews* **85**, (2021).
562 16. Mastronarde, D. N. SerialEM: A Program for Automated Tilt Series Acquisition on
563 Tecnai Microscopes Using Prediction of Specimen Position. *Microscopy and*
564 *Microanalysis* **9**, 1182–1183 (2003).
565 17. Wu, C., Huang, X., Cheng, J., Zhu, D. & Zhang, X. High-quality, high-throughput
566 cryo-electron microscopy data collection via beam tilt and astigmatism-free
567 beam-image shift. *J Struct Biol* **208**, (2019).
568 18. Zheng, S. Q. *et al.* MotionCor2: Anisotropic correction of beam-induced motion for
569 improved cryo-electron microscopy. *Nature Methods* vol. 14 331–332 Preprint at
570 https://doi.org/10.1038/nmeth.4193 (2017).
571 19. Rohou, A. & Grigorieff, N. CTFFIND4: Fast and accurate defocus estimation from
572 electron micrographs. *J Struct Biol* **192**, 216–221 (2015).
573 20. Punjani, A., Rubinstein, J. L., Fleet, D. J. & Brubaker, M. A. cryoSPARC:

algorithms for rapid unsupervised cryo-EM structure determination. *Nat Methods* **14**, 290–296 (2017).

21. Jørgensen, R. *et al.* Two crystal structures demonstrate large conformational changes in the eukaryotic ribosomal translocase. *Nat Struct Mol Biol* **10**, 379–385 (2003).

22. Pettersen, E. F. *et al.* UCSF Chimera—A visualization system for exploratory research and analysis. *J Comput Chem* **25**, 1605–1612 (2004).

23. Emsley, P., Lohkamp, B., Scott, W. G. & Cowtan, K. Features and development of {\it Coot}. *Acta Crystallographica Section D* **66**, 486–501 (2010).

24. Afonine, P. V *et al.* Real-space refinement in {\it PHENIX} for cryo-EM and crystallography. *Acta Crystallographica Section D* **74**, 531–544 (2018).

25. Williams, C. J. *et al.* MolProbity: More and better reference data for improved all-atom structure validation. *Protein Science* **27**, 293–315 (2018).

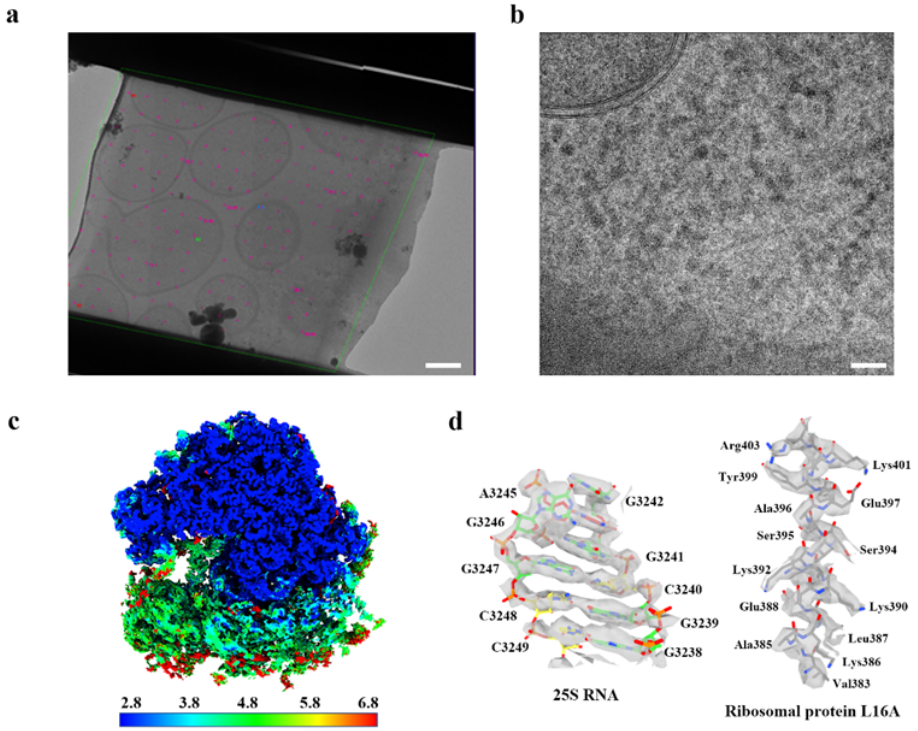

Figure 1. In situ ribosome structure of *S. cerevisiae*. (a) Overview of the cellular lamella, the crosses in magenta indicates the areas for data collection. The scale bar is 1 μm. (b) A micrograph showing the cellular context of *S. cerevisiae*, the scale bar is 50 nm. (c) Local resolution map of averaged ribosome. (d) Well-resolved rRNA bases (left) and ribosomal protein side chains (right).

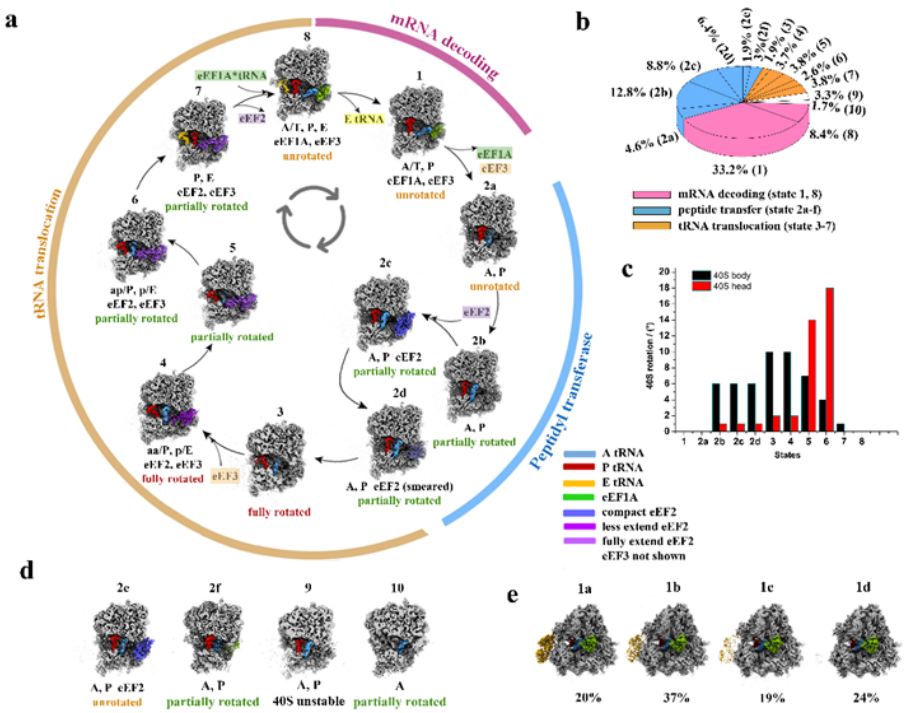

Figure 2. Ribosome conformations and translation elongation cycle. (a) Eleven structures distinguished by elongation factors and tRNAs reconstruct the elongation cycle: mRNA decoding (pink), peptidyl transferase (blue) and tRNA translocation (orange). The rotation states, tRNAs and elongation factors are indicated by colors. (b) The frequencies of occurrence for different states are calculated by the classified particle numbers. States belonging to each process are colored the same as (a). (c) The rotation and swiveling angles of 40S body and head in different states. (d) Four additional structures can't be placed in the sequential cycle. Among them, state 2e is a state belonging to peptide transfer, with non-rotated 40S and compact eEF2 bound, therefore can't be put in the cycle. State 2f may be a mixture of state 2a and state 2b, or an intermediate between the two states. State 9 shows different heterogeneities in 60S and 40S regions, the density quality of tRNAs and 60S are similar, but the 40S presents worse density quality compared to 60S. State 10 contdains only a tRNA in A-site. (e) Four conformations related to eEF3 belong to the "A/T, P" state (state 1), state 1a is the state with stable bound eEF3, state 1b has a little flexibility in eEF3, state 1c show severer flexibility in eEF3 compared to state 1b and state 1d lost connection with eEF3.

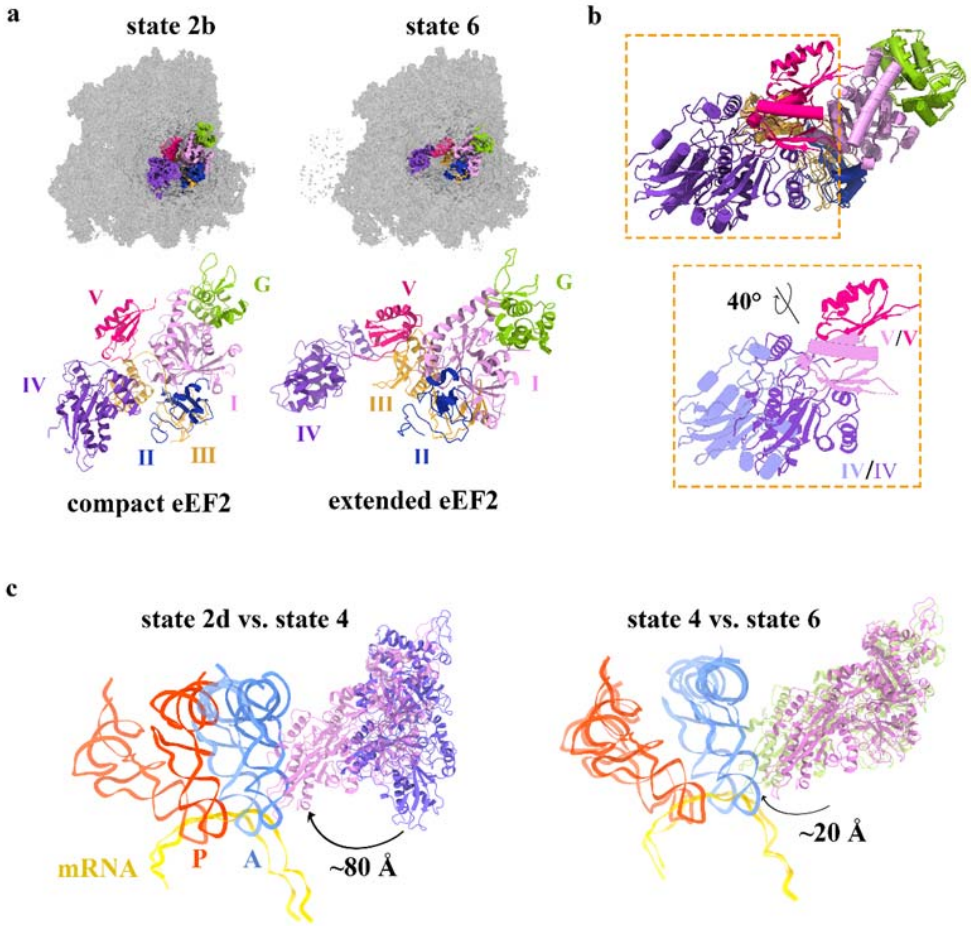

Figure 3. eEF2 and ribosome conformational changes. (a) Overview of the eEF2 bound to ribosomes. The cryo-EM densities of eEF2 are colored differently. Cartoon representations of eEF2 shown in the compact conformation (left) and fully-extended conformation (right), with domains colored the same with densities: domain I (pink), domain II (navy), domain III (orange), domain (purple), domain V (rose red) and domain G (green). (b) Superimposition of the structures of the fully-extended and the compact eEF2. Helices in the fully-extended eEF2 are displayed as cylinders. The main conformational changes appear in the domain and V, which is indicated by a rectangle box. Lower panel recolored the two domains of fully-extended eEF2 with light color to illustrate the overall rotation by about 40 degrees. (c) Overall movement of eEF2 and tRNAs on ribosome. From compact (light purple) to less-extended conformations (pink), domain travels mostly by about 80 Å (left). From less-extended manner to fully-extended manner (light green), domain extends mostly about 20 Å to insert into the A-site on 40S.

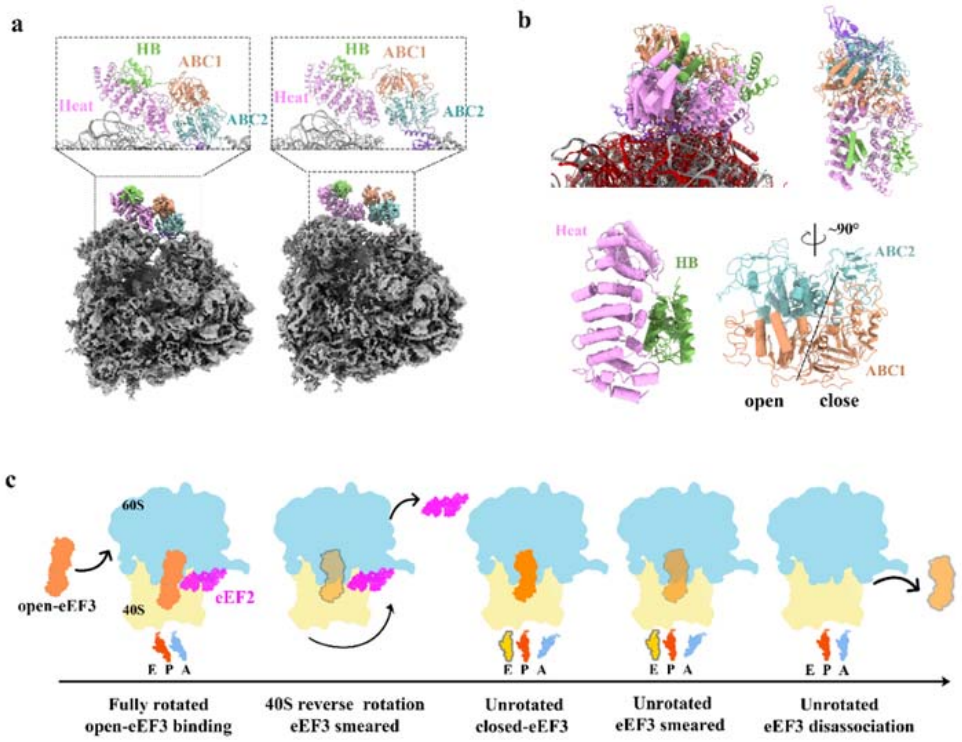

Figure 4. eEF3 binds to and disassociates from ribosome with different conformations. (a) Overview of closed-eEF3 (left) and open-eEF3 (right) complexed with unrotated ribosome and fully-rotated ribosome and zoom illustrating eEF3 of its domains colored: Heat (pink), HB (green), ABC1 (orange) and ABC2 (cyan). (b) Superimposition of structures of closed-eEF3 and open-eEF3 with RNAs colored in red (fully rotated) and gray (unrotated), respectively. Helices in the open-eEF3 are displayed as cylinders. Closed-eEF3 has an overall rotation to open-eEF3 caused by the rotation of 40S (upper right), but the main conformational changes between the two structures appear in the ABC domains. When the heat and HB domains are matched, ABC1 and ABC2 domains have a rotation of about 90 degrees on the axis of heat domain. (c) Binding state of eEF3 varies with the ribosome state. Open-eEF3 binds to fully-rotated ribosome, this binding gets weaker and eEF3 conformation changes to closed-eEF3 during ribosome's reverse rotation. When ribosome just returns back to unrotated state (with or without E-site tRNA), the interaction between closed-eEF3 and ribosome re-stabled, but subsequently closed-eEF3 density gets smeared and disassociates from ribosome before peptide transfer happened. The presence of E-site tRNA does not affect the binding state of eEF3.

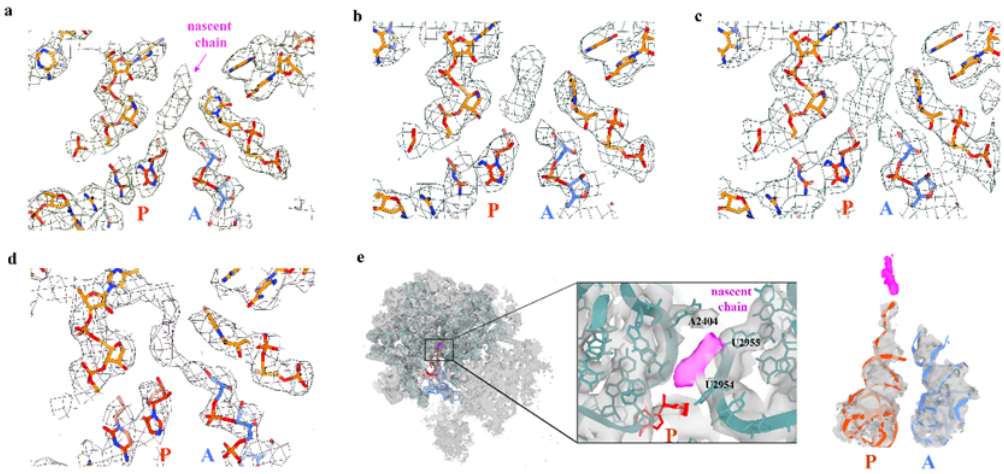

Figure 5. Cryo-EM densities presentation in PTC during Peptidyl transfer. (a) The nascent peptide chain is connected with P-site tRNA (red) and the CCA of A-site tRNA (blue) is accommodated in PTC. The contour level is set as 2.6 RMSD in (a), (b) and (d). (b) Nucleophilic attack breaks the acyl linkage between the carbonyl carbon and P-site tRNA and form peptide bond. The linkage between peptide chain between P-site tRNA becomes weaker compared with (a), thus the chain disconnects with P-site tRNA and A-site tRNA at contour value 2.6 RMSD. (c) The linkages of peptide chain between P-site tRNA and A-site tRNA can be observed at contour value 1.8 RMSD. (d) The peptide chain disconnects with P-site tRNA and is connected to A-site tRNA, indicating that the peptide transfer process is complete. (e) The CCA end of A-site tRNA is smeared in state 2e, and the peptide chain is not connected to neither A-site tRNA nor P-site tRNA. The chain is stabilized by the nucleotides U2954 and U2955 of the 25sRNA in the PTC.